

Improvements in Microstructure and Wear Resistance of Plasma-Sprayed Fe-Based Amorphous Coating by Laser-Remelting

Chaoping Jiang^{1,2} · Hong Chen¹ · Gui Wang² · Yongnan Chen¹ · Yazhe Xing¹ · Chunhua Zhang³ · Matthew Dargusch²

Submitted: 6 November 2016/in revised form: 20 February 2017/Published online: 17 March 2017
© ASM International 2017

Abstract Amorphous coating technology is an attractive way of taking advantage of the superior properties of amorphous alloys for structural applications. However, the limited bonds between splats within the plasma-sprayed coatings result in a typically lamellar and porous coating structure. To overcome these limitations, the as-sprayed coating was treated by a laser-remelting process. The microstructure and phase composition of two coatings were analyzed using scanning electron microscopy with energy-dispersive spectroscopy, transmission electron microscopy, and x-ray diffraction. The wear resistance of the plasma-sprayed coating and laser-remelted coating was studied comparatively using a pin-on-disc wear test under dry friction conditions. It was revealed that the laser-remelted coating exhibited better wear resistance because of its defect-free and amorphous-nanocrystalline composited structure.

Keywords amorphous coating · laser · microstructure · wear

Introduction

Amorphous alloys—also referred to as metallic glasses—are alloys which possess a disordered atomic-scale structure and contain short- to medium-range ordered clusters (Ref 1). Amorphous alloys have attracted scientific and engineering interest for decades, and their importance has been steadily increasing. It has been confirmed that amorphous alloys have new alloy compositions and atomic configurations, which differ from those of conventional crystalline alloys. Their characteristics have facilitated various favorable properties, such as good mechanical properties, useful physical properties, and unique chemical properties, which have not been obtained from crystalline alloys (Ref 2–4). So far, amorphous alloys have been discovered in many alloy systems including Pd-based (Ref 5), Zr-based (Ref 6, 7), Cu-based (Ref 8, 9), Mg-based (Ref 10, 11), Fe-based (Ref 12, 13), Ni-based (Ref 14, 15), Co-based (Ref 16, 17), Pt-based (Ref 18), and Au-based (Ref 19) systems.

There are several possible processes by which to produce amorphous metals, including rapid solidification, physical vapor deposition, solid-state reaction, ion irradiation, and mechanical alloying (Ref 20). To obtain an amorphous phase by rapid solidification, it is essential to suppress the nucleation and growth of a crystalline phase in the supercooled liquid region between the melting temperature (T_m) and the glass transition temperature (T_g). In order to achieve this, the cooling rate of the melt should be greater than the critical cooling rate (R_c). The R_c has been reported to be higher than 10^4 K/s for Fe-based alloys (Ref 21).

Among the various amorphous alloy systems, Fe-based amorphous alloys fabricated by rapid-quenching exhibit excellent tribological properties with low friction

✉ Chaoping Jiang
jcp100415@126.com

¹ School of Materials Science and Engineering, Chang'an University, Xi'an 710061, China

² Centre for Advanced Materials Processing and Manufacturing, School of Mechanical and Mining Engineering, The University of Queensland, St Lucia, QLD 4072, Australia

³ School of Automobile, Chang'an University, Xi'an 710061, China

coefficients and wear rates, showing great potential for applications for parts under severe frictional wear conditions (Ref 22, 23). However, amorphous alloys in general have a very limited plasticity due to a mechanism of heterogeneous deformation, and it is believed that the heterogeneous deformation of the amorphous alloys results in the formation of shear bands (Ref 24, 25). It has been reported that crystalline/amorphous composites featuring microstructures containing crystalline phases dispersed in the amorphous matrix can effectively control the propagation of shear bands (Ref 2, 3); therefore, a significant increase in their plasticity and fracture resistance is achieved (Ref 26). While it is still difficult to produce large sizes of bulk amorphous Fe-based alloys because of the high R_c required, amorphous coatings are much easier to produce and have been extensively studied due to their unique mechanical properties (Ref 27). Miura et al. (Ref. 28) have fabricated Fe-Ni-P-B amorphous and nanocrystalline composite coatings on copper and mild steel using flame spray technology. However, due to a low speed of in-flight particles during flame spraying, the coatings exhibited poor bonding strength and contained lots of pores. To enhance the quality of the coatings, plasma spraying and high-velocity oxygen fuel spraying technologies were used to fabricate Fe-based amorphous coatings (Ref 29). Movahedi produced a Fe-based amorphous feedstock using mechanical alloying and then developed amorphous-nanocrystalline coatings by adjusting the spray parameters of HVOF (Ref 30). Yugeswaran fabricated a high-quality Fe-based amorphous coating through a plasma spraying process, and he has reported that with increasing plasma current, the crystallinity increases and porosity reduces (Ref 31). However, it is difficult to achieve defect-free coatings using thermal spray technology due to the intrinsic porous feature of thermally sprayed coatings (Ref 32).

Laser-remelting with high-power laser irradiation can cause rapid localized heating and melting of the materials. By controlling the scanning speed and power of the laser beam, amorphous and nanocrystalline composite coatings can be acquired to a specified depth because of the fast cooling feature of this process (Ref 33). The coatings with high amorphous proportions prepared by high-power laser irradiation exhibited attractive properties such as low friction, high hardness, and good wear resistance (Ref 34). Several researchers have reported the enhancement of surface properties during laser processing by changing the thermal conditions to obtain desired microstructures within the coating (Ref 35–37).

The aim of the present work is to investigate the effect of the microstructure and phase evolution of amorphous-crystalline composite coatings obtained through laser-remelting of plasma-sprayed coatings. The formation mechanism of the crystalline-amorphous coating and wear

resistance of the two kinds of coatings will also be discussed.

Experimental

Fe-based amorphous powders (Beijing Sangyao Spraying Technology Co., Ltd., China) prepared by gas atomization were used as the feedstock material. The average size of powders was in a range of 30–60 μm and their nominal composition is listed in Table 1.

Substrate specimens with dimensions of 30 (L) \times 15 (W) \times 3 (T) mm were prepared by wire electrode cutting from 1045 mild steel plate. Cylindrical steel rods with dimensions of 6 (D) \times 30 (L) were used for the wear test. Prior to plasma spraying, the specimens were sand-blasted with brown corundum, followed by washing with acetone to clean the surface. The surface roughness of the substrate after sand blasting was $10.8 \pm 1.2 \mu\text{m}$ (R_a). Argon was used as the primary gas, while hydrogen was used as the auxiliary gas. The optimized parameters of the plasma spraying included are as follows: (1) The operational pressures of both argon and hydrogen were 0.7 and 0.68 MPa, respectively; (2) the flow rate of argon was 60 L/min, and that of hydrogen was 6 L/min; (3) argon was used as the powder carrying gas and the feed rate was 10 g/min; (4) the spraying distance was 100 mm; (5) the plasma spray system (ZB-80, Beijing Zhenbang Aerospace Co., Ltd., China) was operated to deposit the coatings at an optimized power level of 25 kW (500 A/50 V); (6) the thickness of the coatings was approximately $250 \pm 5 \mu\text{m}$; and (7) the substrate temperature was controlled to be no more than 75 $^\circ\text{C}$, using compressed air cooling to keep high a cooling rate during deposition.

To eliminate the heave of the coating surface, the as-sprayed coatings were ground by 800 grit quartz abrasive paper. An impulse laser system (HWLW-300A, United Winners Laser Co., Ltd. China) was utilized for laser-remelting under the optimized parameters listed in Table 2. In the remelting process, a continuous flow of argon gas was maintained to prevent oxidation of the molten pool and the substrate was immersed in liquid nitrogen in order to achieve a high cooling rate, as shown in Fig. 1.

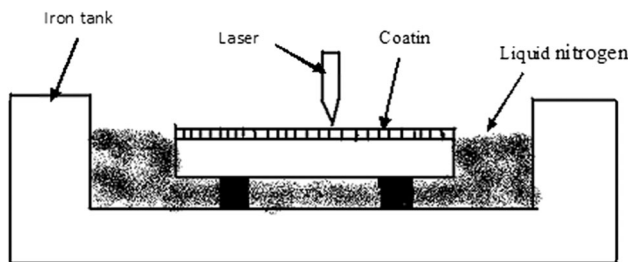
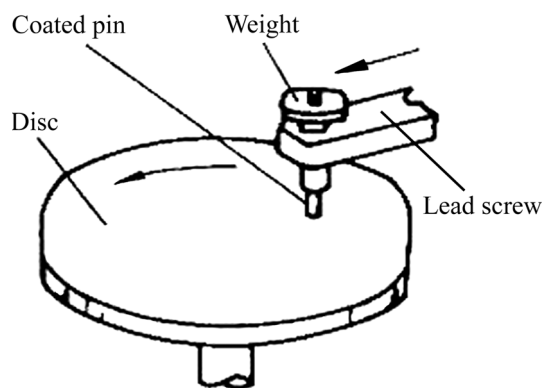
Before the wear and hardness tests, the as-sprayed coating and remelted coating were ground using 1600 grit SiC abrasive paper to achieve a uniform roughness ($R_a = 0.2 \mu\text{m}$). Then, the specimens for the hardness tests

Table 1 Compositions of Fe-based powders

Element	Mo	Cr	Ni	P	Si	B	C	Fe
wt.%	3.4	7.3	2.63	6.34	2.41	0.82	3.84	Bal.

Table 2 Optimized parameters for laser-remelting

Parameters	Laser power, kW	Scan speed, mm/s	Overlapping, %	Fill space, mm	Frequency, HZ
wt. %	2	60	50	1	18

**Fig. 1** Schematic diagram of the laser treatment process**Fig. 2** Schematic diagram of the abrasive wear tester

were polished in order to obtain a surface roughness of $R_a = 0.1 \mu\text{m}$. The surface hardness values of the two coatings were determined using a microhardness tester (HXD-1000TM/LCD, Shanghai Zhongheng Instrument Co., China) with a load of 200 g for 15 s. Ten points were tested along a crossed line on the surface of each coating with an interval distance of $80 \mu\text{m}$. Approximately 5 microhardness readings were taken at each location, and an average value was reported.

Wear properties of the coatings, with and without laser treatment, were evaluated by pin-on-disc testing (ML-10, Xuanhua Material Test Factory, China) under dry sliding conditions at room temperature; the schematic diagram for which is shown in Fig. 2. The coating was fabricated on the one end of a rod-like sample (pin). During the tests, the coated pin slid on a waterproof abrasive paper (with 600 grit quartz particles) mounted on the surface of a steel disc (200 mm in diameter). The wear tests were performed under four applied loads of 0.98, 2.94, 4.9, and 6.86 N. The rotary speed of the disc was 60 r/min. The lead screw, with the pin, moved along the radial direction from the center to the edge of the disc to complete a stroke for 30 s, where the slide distance of one stroke is 8 m. After each stroke, an

Archimedes spiral wear track was formed on the abrasive paper, which was then replaced by a new one for the next stroke. Each sample was run for two strokes during the wear test. After testing, the specimen was cleaned with acetone to remove the loose debris, dried by hot air, and measured with an analytical balance (BS400-WE, Sartorius AG, Germany). Under the same load, five samples were tested and then the mean mass loss value was obtained.

Phase compositions of the as-sprayed coating and laser-remelted coating were determined using x-ray diffraction (XRD, D/max 2500PC, Rigaku, Japan) with monochromatic Cu-K radiation in the range of 20° – 80° (2θ). The detailed structure of the remelted coating was further examined by transmission electron microscopy (TEM, JEM-3010, JEOL, Japan). TEM samples were prepared by electro-polishing using a twin jet polisher. The cross sections and worn surfaces of the coatings were examined using scanning electron microscopy (SEM VEGA II-XMU, TESCAN, Czech) equipped with energy-dispersive x-ray spectrometry (EDS). EDS analysis was conducted on the cross section of the laser-remelted coating to examine the changes in the elements contents. The apparent porosity of the coatings was estimated using the Image Pro Plus version 6.1 software analysis technique. The whole cross sections of coatings were imaged by SEM in backscattered electron mode at 500 magnifications.

Results

Structure of the Coatings

Figure 3(a) shows a typical lamellar structure from the cross-sectional SEM images of the plasma-sprayed coatings. During plasma spraying, molten particles impacted upon the surface of substrate, then deformed, solidified, and transformed into splats. Subsequently, splats piled up upon each other to build up the coating. A clear interface exists between the splats, as marked by arrow 1. Voids and partially melted particles appeared in the coating, as marked by arrows 3 and 2, respectively; some relatively large voids also existed adjacent to those partially melted particles. The apparent porosity of the as-sprayed coating is $4.8 \pm 0.2\%$. In contrast, the cross-sectional SEM image of the laser-remelted coating in Fig. 3(b) showed that no obvious lamellar structure and no voids appeared in the coating, and that the maximum depth of the laser-remelted layer on the coating was about $300 \mu\text{m}$.

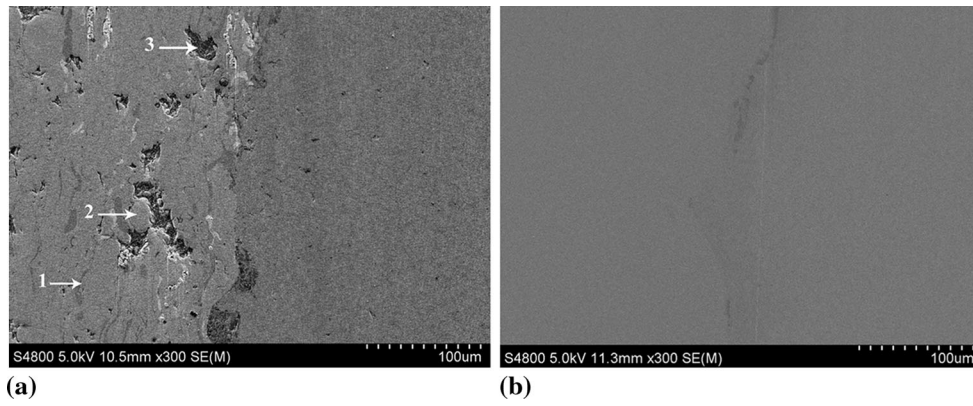


Fig. 3 Cross-sectional SEM images of the coatings (a) as-sprayed and (b) laser-remelted

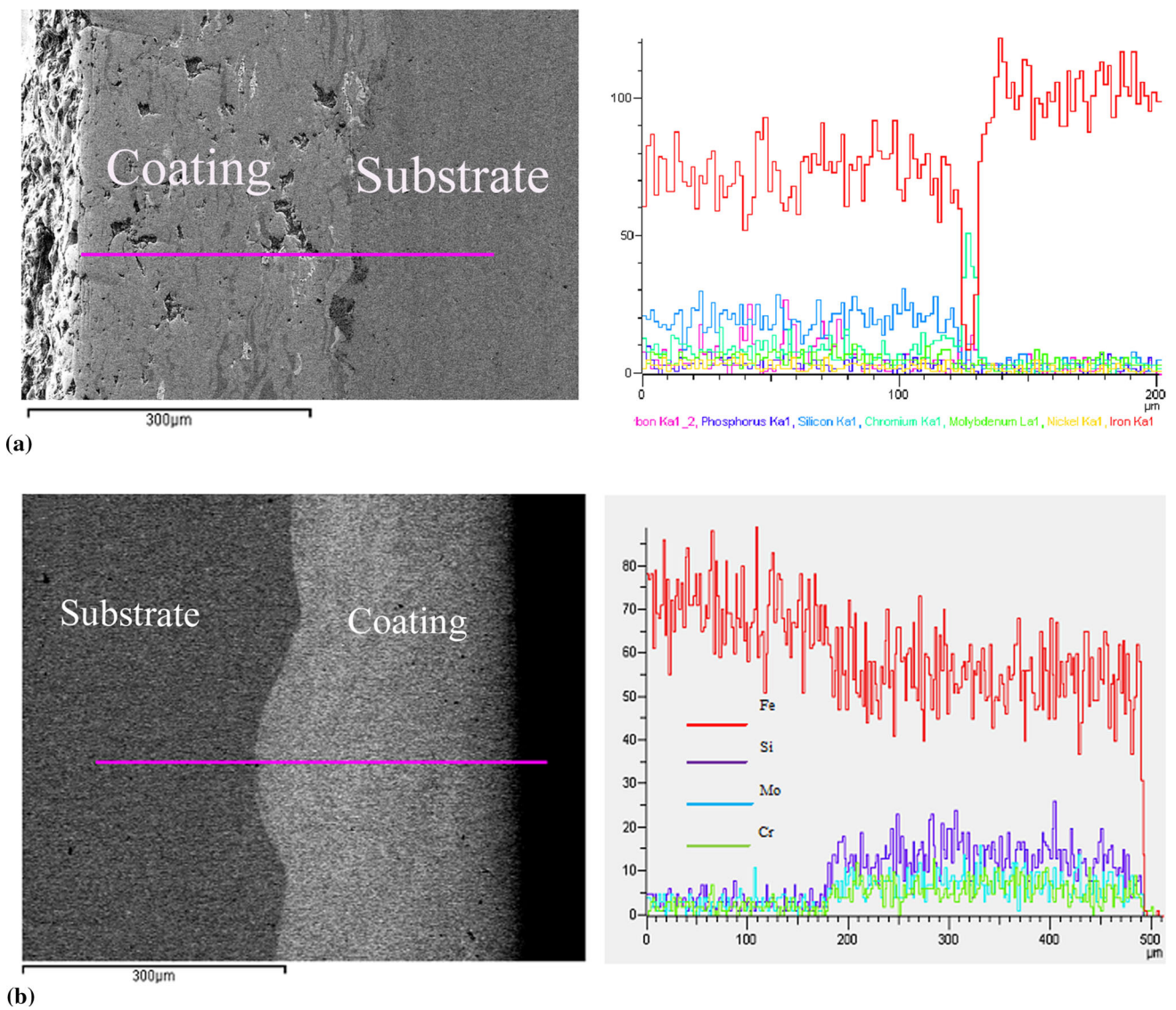


Fig. 4 Cross-sectional SEM and EDS images of the coatings (a) as-sprayed and (b) laser-remelted

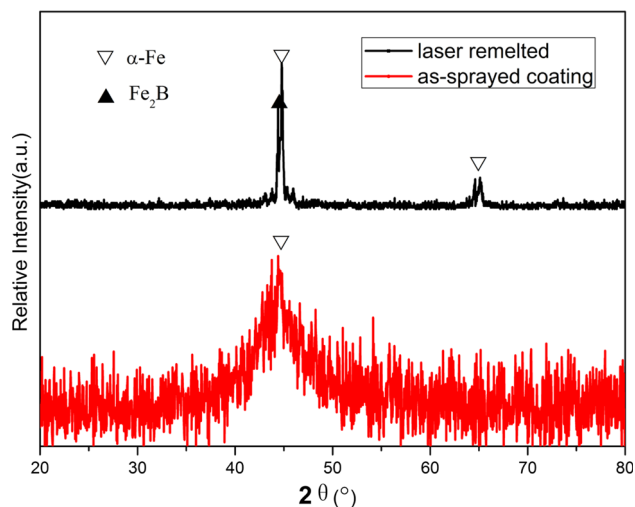


Fig. 5 XRD patterns of as-sprayed and laser-remelted coatings

The elemental distribution along the line across the coating/substrate interface, measured by EDS line scanning, is shown in Fig. 4. The plasma-sprayed coating without laser-remelting treatment only bonds the substrate mechanically (Fig. 4a). As shown in Fig. 4(b), in the EDS line scan patterns from 180 to 250 μm , the content of Fe decreases slowly and, contrary to this, the contents of Cr, Si, and Mo increase continuously. These clearly indicate that in this zone the elements interfused. The depth of the molten pool for the laser-remelting treatment was measured to be about 300 μm , which is larger than the thickness of the as-sprayed coating (250 μm), resulting in a strong metallurgical bonding between the coating and the substrate.

Figure 5 shows XRD patterns of the as-sprayed and laser-remelted coatings. The plasma-sprayed coating is mainly composed of an amorphous phase which is identified by a broad diffraction peak within the range of 40°–50°. The intensity of the diffraction peaks in the plasma-sprayed coating is very low, indicating some nanoscale α -Fe grains appeared in the coating. The coatings obtained through laser-remelting show a fraction of amorphous phases. Some sharp diffraction peaks superimposed on a broad halo pattern were observed, indicating the formation of a mixture of amorphous and crystalline α -Fe and Fe_2B phases. Figure 6 presents the high-resolution TEM micrograph of the laser-remelted coating. It can be seen that the remelted coating shows an amorphous and crystal composite structure, as indicated by the diffraction rings and points. This implies that the amorphous phase of the coating transforms into a crystalline one during the laser-remelting treatment. The continuous laser-remelting process is inclined to form a crystalline phase, as shown in Fig. 7. High cooling rates of the molten pool alloy can lead to the formation of an amorphous phase. When the formed

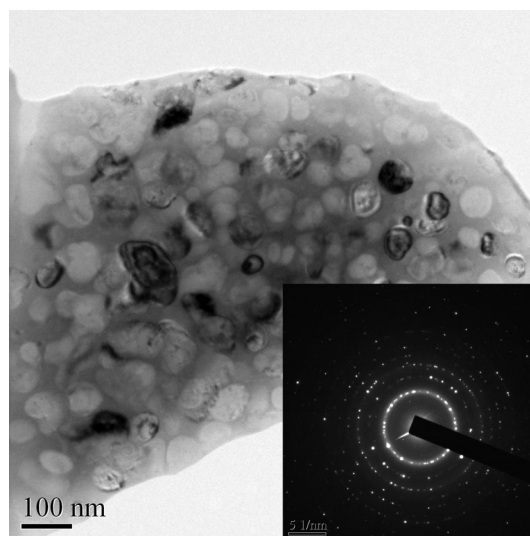


Fig. 6 Bright-field TEM images and corresponding selected area electron diffraction pattern of the laser-remelted coating

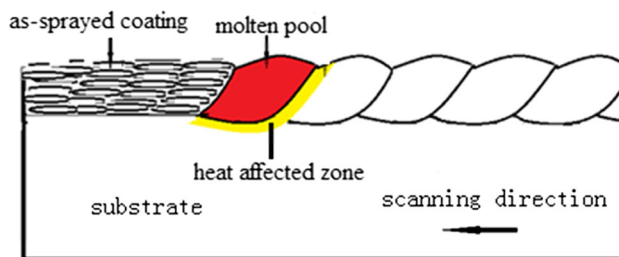


Fig. 7 Schematic diagram of laser-remelting process

amorphous phase is in the heat-affected zone by the subsequent molten pool, a transformation from an amorphous to a crystalline phase occurs because the temperature in the zone can be higher than the onset of the crystallization temperature (Ref 38). The heat-affected zone has also been previously investigated in Matthews' study, in which both Cu-based amorphous and nanocrystalline phases existed in a laser-remelted coating (Ref 34).

Microhardness and Wear Behaviors of Plasma-Sprayed and Laser-Remelted Coatings

The microhardness of the as-sprayed coating is $742.8 \pm 167 \text{ Hv}_{0.2}$. The remelted coating has a higher microhardness ($1182.6 \pm 151.7 \text{ Hv}_{0.2}$) than that of the as-sprayed coating due to its compact structure and formed nanocrystals (Ref 39). The lowest microhardness value of the remelted coating is still higher than the highest microhardness value of the as-sprayed coating. Figure 8 shows the mass loss of the as-sprayed coating and laser-remelted coating after wear testing under the same conditions. It can be seen that the mass losses of both coatings increased linearly with the increase in load. When the load

was up to 6.89 N, the mass loss of the remelted coating was 15.1 mg which is much lower than that of the as-sprayed coating (21.5 mg). The mass loss rate of the remelted coating (10.8 mg/N) was also less than that (18.8 mg/N) of the as-sprayed coating.

In order to investigate the differences in wear mechanism between the as-sprayed coating and the laser-remelted coating, the worn surface morphologies of the coatings tested at 6.89 N normal load were examined by SEM as shown in Fig. 9. Figure 9(a) and (c) shows the worn surface

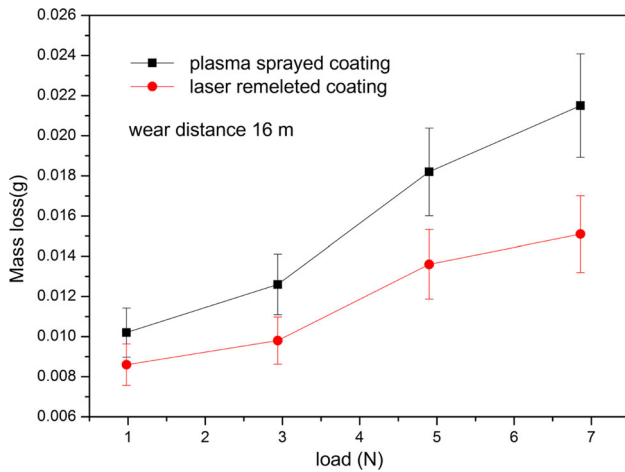


Fig. 8 Mass losses of plasma-sprayed and laser-remelted coatings

morphologies of as-sprayed coatings with different magnifications. It indicates that the major wear mechanisms are abrasion, delamination, splats fracture, and ploughing which formed as hard quartz particles dug into the sliding specimen’s surface and then ploughed out the materials from the groove to the sides. The delaminations and fractured splats can be easily observed in the plasma-sprayed coating due to its lamellar structure and voids content, as marked by arrows in Fig. 9(a) and (c). The debris was worn off from the surface of the coating, leading to mass loss during the process of the wear test. As for the remelted coating, only narrow groove traces without splats, delamination, and fracture were observed on the worn surface, as shown in Fig. 9(b) and (d). The dominant wear mechanism is abrasion and ploughing by plastic deformation.

Discussion

It is well known that the wear behavior of the coatings depends on the microstructure and phase composition. In spraying processes when the splats overlap each other, some voids may be formed due to the insufficient deformation of powder particles (Ref 40). In addition, the splats solidification time is very short: about 10^{-7} to 10^{-6} s, and as such the trapped gas during deposition cannot escape from the molten drops, which also results in the formation

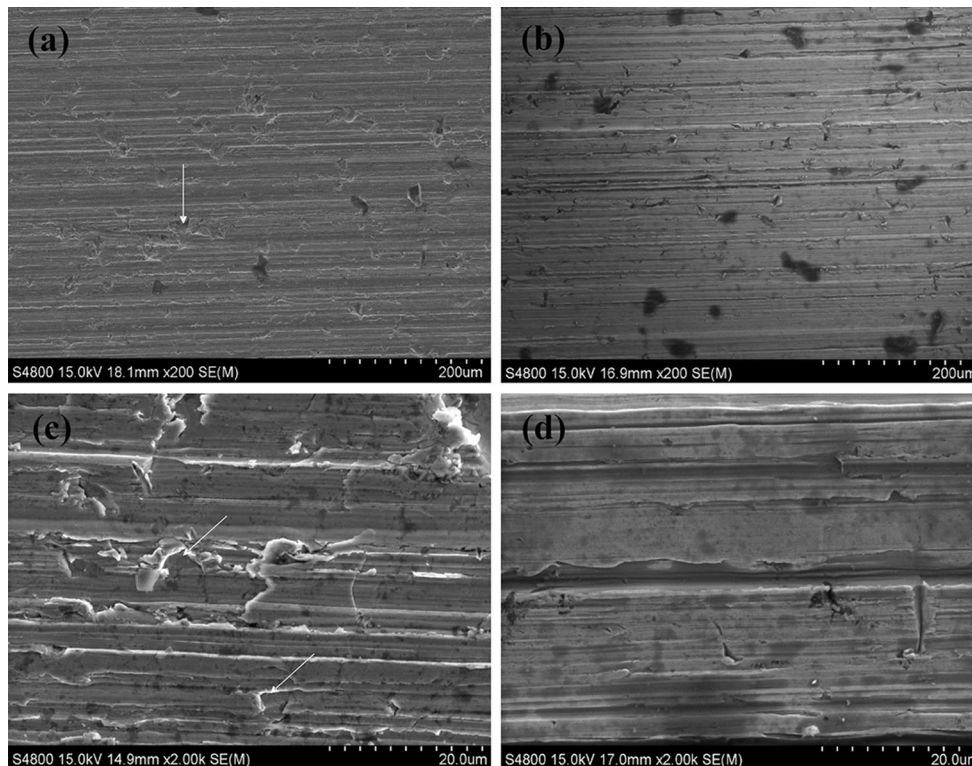


Fig. 9 Wear tracks of the coatings under different magnifications (a), (c) plasma-sprayed coatings (b), (d) laser-remelted coatings

of pores within the coating (Ref 41). During a friction process, the splats of plasma-sprayed coating, which lie around the voids or partial molten particles, are prone to break away from the coating or to fracture because of poor adhesion forces and less support from adjacent splats. The fractured splat tips and deformed splats usually appear in the wear scar of the thermal spray coating under dry conditions (Ref 42). In particular, under high-load conditions, the splats fracture, fragmentation, and delamination become common (Ref 43, 44). Similar behavior has also been observed in Yoon's study on the plasma-sprayed $\text{Fe}_{68.8}\text{C}_7\text{Si}_{3.5}\text{B}_5\text{P}_{9.6}\text{Cr}_{2.1}\text{Mo}_2\text{Al}_2$ amorphous coating (Ref 45).

Compared to the plasma-sprayed coating, the laser-remelted coating showed a more dense and integrated structure. It can be seen that the laser-remelting process completely changes the structure of the as-sprayed coating. The surface hardness of the coating increased greatly because of the existence of nanocrystals and its compact structure in laser processing (Ref 46). The lamellar structures, voids, and unmelted particles were all removed after the laser treatment. Some pores with a diameter of about

2 μm can be observed in the coatings, which are probably a result of the gas entrapped within the molten pool during the laser process. The nanoscale crystals embedded in the amorphous matrix result in increases for both the hardness and the toughness of the laser-remelted coating, subsequently reducing the wear loss (Ref 47). According to recent studies, the probable strengthening mechanism of the laser-remelted coating is that nanocrystals cannot support dislocation pileups, resulting in dislocation-mediated plasticity being inhibited (Ref 48, 49). As a result, the critical stress levels for initiating plasticity will be increased.

The crystals appearing in the laser-remelted coating may be attributed to two factors. Firstly, the depth of the molten pool is more than that of the plasma-sprayed coating. During laser treatment, the substrate alloy close to the substrate-coating interface can be melted, leading to a different chemical composition of the molten pool to the coatings. This changed composition may reduce the amorphous content in the coating (Ref 50). The formation of Fe_2B is due to the great affinity of Fe to boron, which leads to the formation of boride when the amorphous

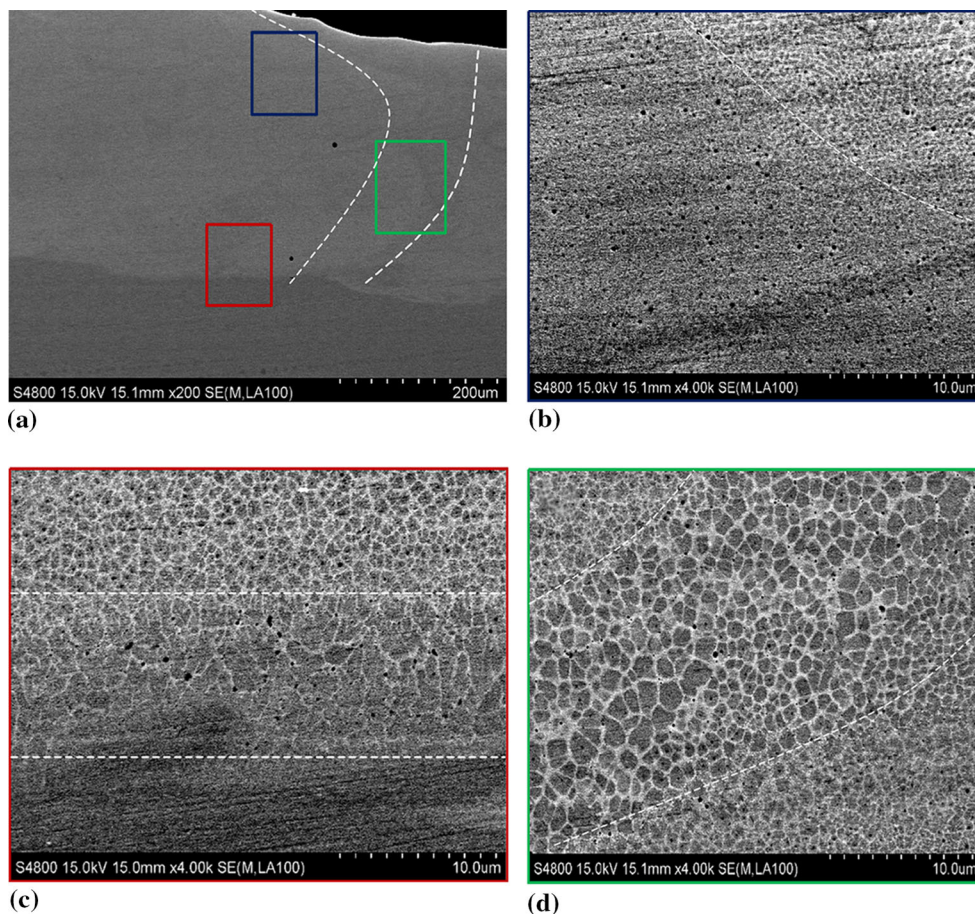


Fig. 10 Cross-sectional SEM images of the remelted coating. (a) overall view, (b) the zone marked by blue frame, (c) the bond zone marked by red frame, (d) the heat-affected zone marked by green frame

coating is heated by laser treatment (Ref 51). Elements B and Fe can easily flock together, which is confirmed by EDS analysis (Ref 51). The presence of these borides has also been found in other researchers' results about laser cladding Fe-based amorphous coatings (Ref 52). Secondly, the crystal particles preferentially form in the heat-affected zone during the continuous laser-remelting process. This can be confirmed by the non-uniform surface hardness of the laser-remelted coating. The smallest hardness value is 150 Hv_{0.2} lower than the average hardness. Big grains appearing in the heat-affected zone have lower microhardness than those in the amorphous phase.

A systematic analysis of the cross-sectional microstructure of a laser-remelted coating was undertaken by SEM, as shown in Fig. 10. Figure 10(a) shows the cross-sectional overview of the laser-remelted Fe-based amorphous coating, and three zones were observed as marked by red, blue, and green blocks. In Fig. 10(b), there are no obvious grains under the dashed line, as marked in zone A. This indicates that an amorphous phase formed in this region because the conditions of the nominal chemical composition and rapid cooling are favorable to the amorphous phase formation. There are also some very small pores with less than 2 μm in size, because the gas present in the as-sprayed coating can hardly get away from the molten pool during the remelting process. Figure 10(c) shows a local magnified image of the remelted coating at the bottom of the molten pool in zone C. The thickness of this zone is about 10 μm, and many large grains have been embedded in the coating. The formation of this zone can be explained in that an increasing amount of the substrate material was melted and mixed with the coating material. In this condition, it is not easy for the amorphous phase to form because of the significant changes in the coating composition from its original nominal chemical composition (Ref 53). Furthermore, some fine pores with larger sizes than the pores in zone A also appear in this region, which can be attributed to the greater entrainment of gases that existed in the defects of the as-sprayed coating. Another reason is that it is very difficult for gas bubbles at the bottom of the pool to travel the whole distance to the outer surface by moving across the viscous, molten metal. In zone B, between two dashed lines, many large equiaxed grains can be observed as shown in Fig. 10(d). This region presents an arc shape, which is in line with the shape of the heat-affected zone in the schematic diagram of the laser-remelting process as shown in Fig. 7. The temperature in this zone can be up to the crystallization temperature of this particular Fe-based alloy; thus, some amorphous phases were converted to crystalline phase (Ref 38). Therefore, an amorphous and nanocrystalline composite coating can be formed by a laser-remelting process.

Conclusions

In this work, an amorphous and nanocrystalline composite coating was fabricated via the laser-remelting treatment of a plasma-sprayed Fe-based amorphous coating. It was demonstrated that the wear resistance of the plasma-sprayed coating can be improved through the laser-remelting process due to a combined amorphous + nanocrystalline structure and defect-free microstructure. The wear mechanism for the plasma-sprayed amorphous coating is dominated by abrasion, delamination, splat fracture, and ploughing under dry friction conditions. In contrast, the wear mechanism of the laser-remelted coating is only dominated by abrasion and ploughing due to the uniform, dense structure, and to the elimination of the voids and lamellar microstructure.

Acknowledgments This work was supported by Natural Science Foundation of Shaanxi Province of China (2016JM5058, 2016JM5059), Natural Nature Science Foundation of China (51301022) and The Special Fund for Basic Scientific Research of Central Colleges, Chang'an University (310831161005, 310831161018, 310831163401).

References

1. M.M. Trexler and N.N. Thadhani, Mechanical Properties of Bulk Metallic Glasses, *Prog. Mater. Sci.*, 2010, **55**, p 759-839
2. W.H. Wang, C. Dong, and C.H. Shek, Bulk Metallic Glasses, *Mater. Sci. Eng. R: Rep.*, 2004, **44**, p 45-90
3. W.L. Johnson, Bulk Glass-Forming Metallic Alloys: Science and Technology, *MRS Bull.*, 1999, **24**, p 42-56
4. J. Schroers, Processing of Bulk Metallic Glass, *Adv. Mater.*, 2010, **22**, p 1566-1597
5. Y. He, R.B. Schwarz, and J.I. Archuleta, Bulk Glass Formation in the Pd-Ni-P System, *Appl. Phys. Lett.*, 1996, **69**, p P1861-P1863
6. Y.J. Sun, D.D. Qu, Y.J. Huang, K.D. Liss, X.S. Wei, D.W. Xing, and J. Shen, Zr-Cu-Ni-Al Bulk Metallic Glasses with Superior Glass-Forming Ability, *Acta Mater.*, 2009, **57**, p 1290-1299
7. Q.S. Zhang, W. Zhang, and A. Inoue, Ni-free Zr-Fe-Al-Cu Bulk Metallic Glasses with High Glass-Forming Ability, *Scr. Mater.*, 2009, **61**, p 241-244
8. B. Huang, H.Y. Bai, and W.H. Wang, Unique Properties of CuZrAl Bulk Metallic Glasses Induced by Microalloying, *J. Appl. Phys.*, 2011, **110**, p 123522
9. P. Jia, H. Guo, Y. Li, J. Xu, and E. Ma, A new Cu-Hf-Al Ternary Bulk Metallic Glass with High Glass-Forming Ability and Ductility, *Scr. Mater.*, 2006, **54**, p 2165-2168
10. Q. Zheng, H. Ma, E. Ma, and J. Xu, Mg-Cu-(Y, Nd) Pseudo-Ternary Bulk Metallic Glasses: The Effects of N_d on Glass-Forming Ability and Plasticity, *Scr. Mater.*, 2006, **55**, p 541-544
11. E.S. Park, H.G. Kang, W.T. Kin, and D.H. Kim, Effect of Ag Addition on the Glass-Forming Ability of Mg-Cu-Y Metallic Glass Alloys, *J. Non-Cryst. Solids*, 2001, **279**, p 154-160
12. S.J. Pang, T. Zhang, K. Asami, and A. Inoue, Synthesis of Fe-Cr-Mo-C-B-P Bulk Metallic Glasses with High Corrosion Resistance, *Acta Mater.*, 2002, **50**, p 489-497
13. Q. Li, J. Li, P. Gong, K. Yao, J. Gao, and H. Li, Formation of Bulk Magnetic Ternary Fe₈₀P₁₃C₇ Glassy Alloy, *Intermetallics*, 2012, **26**, p 62-65

14. J.H. Na, M.D. Demetriou, M. Floyd, A. Hoff, G.R. Garrett, and W.L. Johnson, Compositional Landscape for Glass Formation in Metal Alloys, *PNAS*, 2014, **111**, p 9031-9036
15. Y. Zeng, N. Nishiyama, and A. Inoue, Formation of a Ni-Based Glassy Alloy in Centimeter Scale, *Mater. Trans.*, 2007, **48**, p 1355-1358
16. J. Wang, R. Li, R. Xiao, and T. Xu, Compressibility and Hardness of Co-Based Bulk Metallic Glass: A Combined Experimental and Density Functional Theory Study, *Appl. Phys. Lett.*, 2011, **99**, p 151911
17. Q. Man, H. Sun, Y. Dong, B. Shen, H. Kimura, A. Makino, and A. Inoue, Enhancement of Glass-Forming Ability of CoFeBSiNb Bulk Glassy Alloys with Excellent Soft-Magnetic Properties and Superhigh Strength, *Intermetallics*, 2010, **18**, p 1876-1879
18. T. Zhang and A. Inour, Bulk Glassy Alloys with Low Liquidus Temperature in Pt-Cu-P System, *Mater. Trans.*, 2003, **44**, p 1143-1146
19. W. Zhang, H. Guo, M.W. Chen, Y. Saotome, C.L. Qin, and A. Inoue, New Au-Based Bulk Glassy Alloys with Ultralow Glass Transition Temperature, *Scr. Mater.*, 2009, **61**, p 744-747
20. M.I. Ojovan and W.B.E. Lee, Connectivity and Glass Transition in Disordered Oxide Systems, *J. Non-Cryst. Solids*, 2010, **356**(44-49), p 2534-2540
21. C. Suryanarayana, *Non-equilibrium Processing of Materials*, Pergamon, New York, 1999
22. K. Miyoshi and D.H. Buckley, Microstructure and Surface Chemistry of Amorphous Alloys Important to Their Friction and Wear Behavior, *Wear*, 1986, **110**, p 295-313
23. Kishore, U. Sudarsan, N. Chandran, and K. Chattopadhyay, On the Wear Mechanism of Iron and Nickel Based Transition Metal-Metalloid Metallic Glasses, *Acta Metall.*, 1987, **35**, p 1463-1473
24. C.A. Schuh, T.C. Hufnagel, and U. Ramamurty, Mechanical Behavior of Amorphous Alloys, *Acta Mater.*, 2007, **55**, p 4067-4109
25. E. Axinte, Metallic Glasses from “Alchemy” to Pure Science: Present and Future of Design, Processing and Applications of Glassy Metals, *Mater. Des.*, 2012, **35**, p 518-556
26. F. Abdeljawad, M. Fontus, and M. Haataja, Ductility of Bulk Metallic Glass Composites: Microstructural Effects, *Appl. Phys. Lett.*, 2011, **98**, p 031909-1-3
27. J.B. Cheng, X.B. Liang, Z.H. Wang, and B.S. Xu, Dry Sliding Friction and Wear Properties of Metallic Glass Coating and Martensite Stainless Coating, *Tribol. Int.*, 2013, **60**, p 140-146
28. H. Miura, S. Isa, and K. Omuro, Production of Amorphous Iron-Nickel Based Alloys by Flame-Spray Quenching and Coatings on Metal Substrates, *Mater. Trans. JIM.*, 1984, **25**, p 284-291
29. V. Varadaraajan, R.K. Guduru, and P.S. Mohanty, Synthesis and Microstructural Evolution of Amorphous/Nanocrystalline Steel Coatings by Different Thermal Spray Processes, *J. Therm. Spray Technol.*, 2013, **22**, p 452-462
30. B. Movahedi, M.H. Enayati, and C.C. Wong, Structural and Thermal Behavior of Fe-Cr-Mo-P-B-C-Si Amorphous and Nanocrystalline HVOF Coatings, *J. Therm. Spray Technol.*, 2010, **19**, p 1093-1099
31. S. Yugeswaran and A. Kobayashi, Metallic Glass Coatings Fabricated by Gas Tunnel Type Plasma Spraying, *Vacuum*, 2014, **11**, p 177-182
32. A. Kobayashi, S. Yano, H. Kimura, and A. Inoue, Fe-Based Metallic Glass Coatings Produced by Smart Plasma Spraying Process, *Mater. Sci. Eng. B*, 2008, **148**, p 110-113
33. D.T.A. Matthews, V. Ocelík, D. Branagan, and J.Th.M. de Hosson, Laser Engineered Surfaces from Glass Forming Alloy Powder Precursors: Microstructure and Wear, *Surf. Coat. Technol.*, 2009, **2039**, p 1833-1843
34. D.T.A. Matthews, V. Ocelík, and J.Th.M. de Hosson, Tribological and Mechanical Properties of High Power Laser Surface-Treated Metallic Glasses, *Mater. Sci. Eng. A*, 2007, **471**, p 155-164
35. S. Katakam, J.Y. Hwang, S. Paital, R. Banerjee, H. Vora, and N.B. Dahotre, In Situ Laser Synthesis of Fe-Based Amorphous Matrix Composite Coating on Structural Steel, *Metall. Mater. Trans. A*, 2012, **43**, p 4957-4966
36. E. Forozmehr and R. Kovacevic, Thermo-Kinetic Modeling of Phase Transformation in Laser Powder Deposition, *Metall. Mater. Trans. A*, 2009, **40**, p 1935-1943
37. S. Katakam, S. Santhanakrishnan, and N.B. Dahotre, Fe-Based Amorphous Coatings on AISI, 4130 Structural Steel for Corrosion Resistance, *Process. Technol.*, 2012, **64**, p 1247-1259
38. W.W. Liu, X. Lin, G.L. Yang, H.O. Yang, W.D. Huang, and J.F. Li, Crystallization Behavior of Amorphous Heat Affected Zone of Zr₅₅Al₁₀Ni₅Cu₃₀ Alloy by Pulse Laser Remelting, *Chin. J. Lasers*, 2010, **37**, p 2104-2111
39. D.J. Branagan, M. Breitsameter, B.E. Meacham, and V. Belashchenko, High Performance Nanoscale Composite Coatings for Boiler Applications, *J. Therm. Spray Technol.*, 2005, **14**, p 196-204
40. X.B. Zhao and Z.H. Ye, Microstructure and Wear Resistance of Molybdenum Based Amorphous Nanocrystalline Alloy Coating Fabricated by Atmospheric Plasma Spraying, *Surf. Coat. Technol.*, 2013, **228**, p 266-270
41. Z.S. Li, Z.D. Liu, Y.T. Wang, and Y. Wang, Fe-Based Amorphous Composite Coating Prepared by Plasma Remelting, *Adv. Mater. Sci. Eng.*, 2015, **2015**, p 1-6
42. A. Edrisky, T. Perry, Y.T. Cheng, and A.T. Alpas, Wear of Thermal Spray Deposited Low Carbon Steel Coatings on Aluminum Alloys, *Wear*, 2001, **251**, p 1023-1033
43. A. Edrisky, T. Perry, and A.T. Alpas, Wear Mechanism Maps for Thermal-Spray Steel Coatings, *Metall. Mater. Trans. A*, 2005, **36A**, p 2737-2750
44. G. Bolelli, B. Bonferroni, J. Laurila, L. Lusvarghi, A. Milanti, K. Niemi, and P. Vuoristo, Micromechanical Properties and Sliding Wear Behaviour of HVOF-Sprayed Fe-Based Alloy Coatings, *Wear*, 2012, **276-277**, p 29-47
45. S.H. Yoon, J.H. Kim, B.D. Kim, and C.H. Lee, Tribological Behavior of B₄C Reinforced Fe-Based Bulk Metallic Glass Composite Coating, *Surf. Coat. Technol.*, 2010, **205**, p 1962-1968
46. T. Fu, F.X. Ye, H.H. Wei, and L. Cui, Laser Surface Remelting of Fe-Based Alloy Coating Deposited by APS, *Rare Metal Mater. Eng.*, 2012, **41**(S1), p 407-413
47. J.C. Huang, J.P. Chu, and J.S.C. Jang, Recent Progress in Metallic Glasses in Taiwan, *Intermetallics*, 2009, **17**, p 973-987
48. D.J. Branagan, W.D. Swank, D.C. Haggard, and J.R. Fincke, Wear-Resistant Amorphous and Nanocomposite Steel Coatings, *Metall. Mater. Trans. A*, 2001, **32**, p 2615-2621
49. J.R. Weertman, D. Farkas, K. Hemker, H. Kung, M. Mayo, R. Mitra, and H. Van Swygenhoven, Structure and Mechanical Behavior of Bulk Nanocrystalline Materials, *Mater. Res. Soc. Bull.*, 1999, **24**, p 44-50
50. H. Yoshioka, K. Asami, A. Kawashima, and K. Hashimoto, Laser-Processed Corrosion-Resistant Amorphous NiCrPB Surface Alloys on a Mild Steel, *Corros. Sci.*, 1987, **27**, p 981-995
51. P.L. Zhang, H. Yan, C.W. Yao, Z.G. Li, Z.S. Yu, and P.Q. Xu, Synthesis of Fe-Ni-B-Si-Nb Amorphous and Crystalline Composite Coatings by Lasercladding and Remelting, *Surf. Coat. Technol.*, 2011, **206**, p 1229-1236
52. P. Gargarella, A. Almeida, R. Vilar, and C.S. Kiminami, Formation of Fe-Based Glassy Matrix Composite Coatings by Laser Processing, *Surf. Coat. Technol.*, 2014, **240**, p 336-343
53. A. Inoue, Bulk Amorphous and Nanocrystalline Alloys with High Functional Properties, *Mater. Sci. Eng. A*, 2001, **304**, p 1-10